Structural Characteristics of Natural Minerals of Gas Hydrates

M. Yousuf,[1] S.B. Qadri,[2] D.L. Knies,[2] K.S. Grabowski,[2] R.B. Coffin[2]
[1]The George Washington University, Washington, DC, U.S.A.
[2]U.S. Naval Research Laboratory, Washington, DC, U.S.A.

Introduction

Laboratory synthesis of gas hydrates typically involves rocking or vigorously shaking the reactants in a pressure-vessel. The reaction has been found to be slow, and ice crystals are commonly added to initiate the reaction. In contrast, gas hydrate formation in the ocean does not involve shaking, and ice crystals are not part of the natural deep-seawater environment. Therefore, laboratory experiments carried out to date have not been able to simulate natural processes. Gas hydrates are believed to form by migration of natural gases from beneath the seafloor along the natural faults, followed by precipitation or crystallization when the rising gas stream contacts cold seawater at pressures of several tens of MPa [1-5].

The crystal growth parameters and the reactants in nature and in the laboratory are often different; hence, it is logical to assume that there is a fair chance of obtaining different products in the two cases. For instance, laboratory experiments can be controlled in idealized conditions so as to achieve a clathrate hydrate of natural gas in a truly single structure-type [6-10], but in nature, this can rarely be possible. This is evidently so since the crystalline states obtained in the seafloor are functions of the (1) type and concentration of natural gases present and their migration rates, (2) temperature and pressure of the seafloor water and the concentration of nonwater bodies, and (3) prevailing hydrodynamics and other variables of the seafloor water environment.

Gas hydrates or clathrate hydrates of natural gases are solidlike minerals formed at low temperature and high pressure by van der Waals forces between gas and water molecules, with the host water molecules forming molecular cages that confine the guest gas molecules through their mutual electrostatic interaction. Hydrates contain natural gases, such as hydrocarbons, that glue themselves inside the water-molecule cages.

Although clathrate hydrates of natural gases contain hydrocarbons that are colorless, not all of them are milky white like snow. For instance, the hydrates from the Gulf of Mexico are richly colored in shades of yellow, orange, or even red, whereas the samples from Cascadia Margin are almost milky white. Though no definite consensus has been reached on the origin of the coloration of the hydrates, the presence of oil, bacteria, and minerals plays a role. In the ocean, gas hydrates, composed dominantly of methane, are a common constituent of the shallow marine geosphere and occur both as deep sedimentary structures and as outcrops on the ocean floor.

Natural gas hydrates occur globally in marine sediments, in permafrost regions, and in the continental ice sheets. Their formation depends on the presence of sufficiently high concentrations of natural gases, such as methane and higher hydrocarbons, an elevated pressure, and a low temperature. Methane is largely a product of the fermentative decomposition of organic matter or of the bacterial CO_2 reduction in sediments. Thermocatalytic conversion of organic matter in the deeper subsurface can be another equally important source of methane and higher hydrocarbons. In this case, methane may migrate from the deeper sources into the hydrate stability zone [11]. Large hydrate deposits are found along the continental margins, and their formation is favored by rapid sedimentation and high concentrations of sedimentary organic matter. On land, the existence of stable methane hydrates in permafrost regions is probably the outcome of natural migration of gases from deeper hydrocarbon reservoirs. Methane hydrates are also known from polar ice sheets, where they form at depth as a result of air inclusions [12].

Hydrocarbons captured in natural minerals of gas hydrates show a preponderance of methane [13-15]. In terms of their ability to react with water and on the basis of their sizes, the condensed matter states of hydrophobic (hydrocarbon) gas molecules with water are classified into five types [16-20]. (1) The smallest guest atoms and molecules, such as hydrogen, helium, and neon (molecular diameter d of <3.5 Å), are capable of forming solid solutions based on ice Ih or, at high pressure, hydrates based on ice II and ice Ic. (2) Guest molecules with somewhat larger diameters, such as argon, krypton, oxygen, and nitrogen (3.5 Å ≤ d ≤ 4.2 Å), form, at relatively low pressure, hydrates with structure II (abbreviated as sII), an fcc structure with space group *Fd3m*. The unit cell contains 8 hexakaidecahedral H cavities ($5^{12}6^4$, a 16-face polyhedron consisting of 12 regular pentagons and 4 regular hexagons) and 16 pentagonal-dodecahedral D cavities (5^{12}, a 12-face polyhedron constituted by regular pentagons) and is occupied by the guest molecules [Fig. 1(a)]. (3) Guest molecules such as H_2S, SO_2, CO_2, Xe, C_2H_6, and others satisfying the criterion 4.3 Å ≤ d ≤ 5.8 Å stabilize hydrate structure I (abbreviated as sI), a simple cubic structure having space group *Pm3n*. The unit cell consists of 2 D cavities and 6 tetrakaidecahedral T cavities ($5^{12}6^2$, a 14-face polyhedron having 12 regular pentagons and

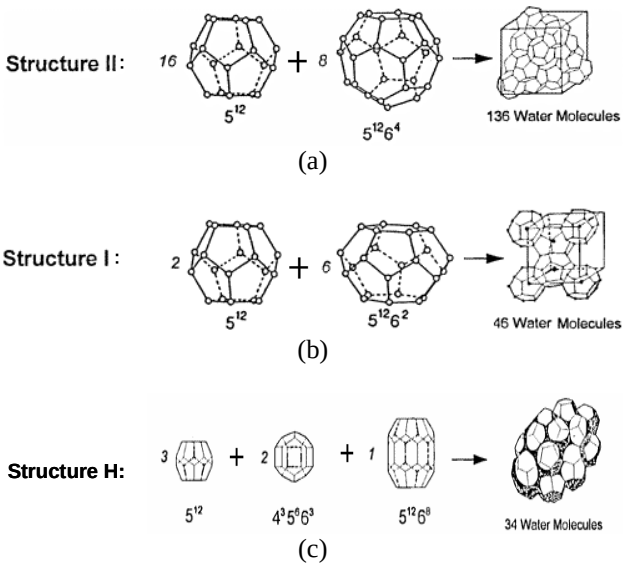

FIG. 1. Unit cells of hydrate structures II (a), I (b), and H (c). The building blocks are in the form of cages formed by water molecules. While structures I and II have two types of cages, structure H has three types of cages.

2 regular hexagons) [Fig. 1(b)]. (4) Guest molecules having the diameter range 5.8 Å ≤ d ≤ 7.2 Å form sII, in that only the H cavities are occupied, whereas the D cavities are unoccupied. (5) In those cases where the guest molecules are very large (e.g., methylcyclohexane, admantane), a new structure called structure H (abbreviated as sH) is formed; this is a simple hexagonal structure with space group *P6/mmm*. In this structure, the unit cell consists of 3 types of cavities, namely 3 regular dodecahedral D cavities, 2 irregular dodecahedral D′ cavities ($4^35^66^3$, an irregular 12-faced polyhedron constituted by joining 3 tetrahedrons, 6 pentagons, and 3 hexagons), and 1 regular icosahedral E cavity ($5^{12}6^8$, a 20-face polyhedron composed of 12 regular pentagons and 8 regular hexagons) [Fig. 1(c)]. It has been recognized that the structure H is stable only in the presence of a helfgas (i.e., help gas) such as methane occupying the D and D′ cavities.

The work presented in this paper was undertaken in the context of the study of clathrate hydrates of natural gases collected from diverse geographic locations in the Pacific, Atlantic, and Arctic Oceans. Attention focused on structural investigations of the natural minerals of the clathrate hydrates because (1) structural information is of prime importance in designing and developing the most appropriate and economically viable technology to tap this vast frozen energy resource from the seafloor; (2) to the best of our knowledge, structural data on these natural minerals are not available; and (3) laboratory experiments carried out to date have not been able to simulate the true natural processes driving the formation of hydrates.

Methods and Materials

Using the Department of Navy vessels, clathrate hydrates of natural gases were collected from five specific locations: (1) Texas-Louisiana Shelf in the Gulf of Mexico, (2) Nankai Trough off the eastern coast of Japan, (3) Blake Ridge in the northwestern Atlantic Ocean, (4) Cascadia Margin in the northeastern Pacific Ocean, and (5) Haakon-Mosby Mud Volcano in the Norwegian-Greenland Sea. During submarine dives, the naturally occurring gas hydrates were recovered from a depth of ~600 m. Hydrate masses were transferred into plastic bags and placed inside an LN_2 Dewar flask for preserving them in their natural state.

A flat and sturdy metallic ~30 × 30-cm platform was maintained close to LN_2 temperature. A pestle-mortar combination kept on the platform was used to prepare a very fine powder of the natural hydrate drawn from the LN_2 Dewar flask. A fine ≤200-μm wire-mesh was used to filter the fine powder from the rest of the samples. An aluminum piston-cylinder assembly (with an inner diameter of 12 mm and length of 25 mm capable of sustaining pneumatic pressure up to ~100 MPa) was packed with the sample and transferred quickly to a closed-cycle refrigerator (CCR) mounted on the diffractometer system at BESSRC beamline station 11-ID-D at the APS. The 11-ID-D beamline has a modified standard BESSRC double-crystal monochromator with a 4.0- to 40-keV energy range that uses a Si(220) crystal with a 20-mm fixed offset. Both crystals are cryo-cooled. The beam was focused by using a Pt-coated 2.8-mrad incident angle torroidal mirror [21]. The CCR was capable of maintaining sample temperatures from 80 to 300K. Pressure and temperature stabilities of the setup used were observed to be 0.01 MPa and 1K, respectively. Two thermocouples, one each at the ends of the pressure cell, were used to monitor the temperature variation across the sample. The pressure cell was allowed to attain steady state such that the temperature difference between the two thermocouples was less than 3K. A trade-off among achieving the highest resolution, largest interplanar spacing, and highest signal-to-noise ratio led us to fix the energy of the incident beam at 25 keV (λ = 0.49592 Å).

First, blank cell experiments were performed to find out the peak positions from aluminum. Since no aluminum peak was observed in the diffraction angle range, $1.5° \le 2\upsilon \le 30°$, all the experiments were performed in the 2υ range. To calibrate the precision and the accuracy of the diffractometer, x-ray powder standards such as Al, Al_2O_3, and ice were loaded inside the pressure cell, and powder diffraction measurements were done. The

resolution in the lattice parameter was observed to be ~10^{-4} Å, and the accuracy was observed to be better than 10^{-3} Å.

To obtain a high resolution and a good signal-to-noise ratio, x-ray diffraction data were acquired by using a scintillation counter detector placed at a distance of ~300 mm from the sample. The $\Delta(2\upsilon)$ step was set at 0.01°, and the data were collected at each point for 3 seconds in the diffraction range $1.5° \leq 2\upsilon \leq 30°$. After the sample pressure was set, the temperature was varied from 90 to 300K. High-purity nitrogen gas was used to pressurize the sample, and the pressure was changed from 4 to 80 MPa.

Accurate 2υ values and the intensity of all the discernible powder diffraction peaks (from a given data set) were obtained by using XFIT, a peak profile-fitting program. We found that the majority of the diffraction peaks fitted well with the pseudo-Voigt distribution, while some peaks required Gaussian and Lorenzian fits. The diffraction data sets were analyzed by using XRDA, a least squares fitting program. The observed peaks were identified with ice Ih and with the gas hydrate structures, namely, sI, sII, and sH. The intensity calculations were performed for ice Ih, sII, sI, and sH, and a search match was made to identify the origin of a diffraction peak. Pertinent inputs to the structure refinements were the lattice parameter(s) taken from the XRDA output; the symmetry positions on the basis of those obtained from nuclear magnetic resonance (NMR); and the positions of oxygen, half-hydrogen, carbon, and hydrogen atoms taken from the acceptable single-crystal x-ray and neutron diffraction literature data. The covalent radii were used throughout the refinement. To improve the intensity match with the experimentally obtained data, atomic positions were varied. The refinement steps were carried on until the best agreement with the observed intensity data was obtained.

Results

First we very briefly describe the hydrocarbon composition and the stable carbon isotope data for the hydrate minerals. Since formation, stability, and dissociation energy of hydrates are functions of biological, chemical, and physical conditions, we performed these two measurements. The hydrocarbon composition data are presented in Table 1. Note that the hydrate minerals consist of a broad range of gases. The stable carbon isotope analysis for hydrocarbons (CH_4 to C_4H_{10}) and CO_2 indicates that in the samples from the Gulf of Mexico and Haakon Mosby Mud Volcano, the value of $\delta^{13}C$ in CH_4 is in the range of -60 to -50, implying that these minerals have a biogenic origin. Representative structural results on natural minerals of gas hydrates obtained from three geographical locations are presented below.

Hydrates of Cascadia Margin, Northeastern Pacific Ocean

The natural minerals collected from the northern Pacific Ocean play were observed to contain a significant concentration of methane traced to a biogenic origin. A typical diffractogram (T = 150K) is shown in Fig. 2. Table 2 lists the experimental d-spacings. The lattice parameters for ice Ih are a = 4.5115 ±0.0068 Å and c = 7.3566 ±0.0001 Å and that for the clathrate hydrate in sI is a = 11.9132 ±0.0235 Å. The major structure of the clathrate hydrates of natural gases samples obtained from the Cascadia Margin is cubic, and the space group is $Pm3n(O_h^3)$. Note that the natural clathrates from the Pacific seafloor collected by using the research cruise ship

TABLE 1. Hydrocarbon content in hydrate samples from the Texas-Louisiana Shelf in the Gulf of Mexico and the Haakon-Mosby Mud Volcano in the Norwegian Greenland Sea. Bush Hill and Green Canyon are located in the Gulf of Mexico. Yellow hydrates have petroleum present between the clathrate structures.

	Hydrocarbon composition (%)						
Sample	C_1	C_2	C_3	*i*-C_4	C_4	C_5	C_6
Bush Hill	29.7	15.3	36.6	9.7	4.0	3.2	1.6
Bush Hill White	72.1	11.5	13.1	2.4	1.0	0.0	0.0
Bush Hill Yellow	73.5	11.5	11.6	2.0	1.0	0.1	0.0
Green Canyon White	66.5	8.9	15.8	7.2	1.4	0.1	0.1
Green Canyon Yellow	69.5	8.6	15.2	5.4	1.2	0.0	0.0
Haakon-Mosby Mud Volcano	99.5	0.1	0.1	0.1	0.1	0.0	0.1

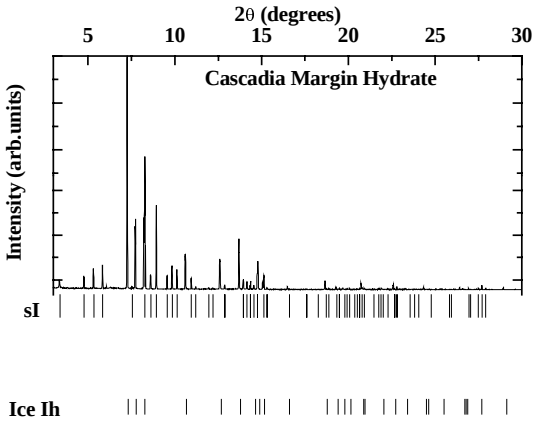

FIG. 2. Powder diffraction pattern for the hydrate sample of the Cascadia Margin. Major constituents are ice Ih and hydrate sI.

SONNE 110 were observed to contain sI, and the sample was found to contain 97.4% CH_4, 2.6% H_2S, and traces of CO_2, C_4H_6, and C_3H_8 [22].

Hydrates of Bush Hill, Gulf of Mexico

Jolliet field of Green Canyon 184 is an example of the direct association between an oil accumulation and thermogenic gas hydrate. Oil and gas are trapped in Pleistocene-Pliocene reservoir sands at a depth of approximately 2-3 km. The Bush Hill gas hydrate site on GC185 occurs at the surface trace of a hydrocarbon-charged antithetic fault, 27° 47.5′ N and 91° 30.5′ W, near Jolliet Field at a depth in water of about 540 m. The natural mineral was collected off the Southwest U.S. Coast. This Gulf of Mexico mineral has been analyzed and found to contain 72-74% methane with the rest being higher hydrocarbons (Table 1). A typical diffractogram (T = 150K) is shown in Fig. 3. Table 3, at the end of the report, lists the experimental d-spacings. The lattice parameters for ice Ih are a = 4.5047 ±0.00037 Å and c = 7.2412 ±0.0001 Å. The lattice parameter of sII is a = 17.0888 ±0.0004 Å. Though we observe that the Bush Hill samples consist mostly of sII and ice Ih, there are several peaks that could have an origin in sI (a = 11.7346 ±0.0300 Å) and sH (a = 11.4496 ±0.3324 Å and c = 9.7064 ±0.0330 Å) (see Table 3).

Hydrates of Green Canyon, Gulf of Mexico

The Green Canyon, Gulf of Mexico, minerals have been analyzed to contain 66% to 70% methane with the rest being higher hydrocarbons, especially ethylene and cyclohexane. A typical diffractogram (T = 150K) is shown in Fig. 4. Table 4, at the end of the report, lists the experimental d-spacings. The lattice parameters for ice Ih are a = 4.5170 ±0.00032 Å and c = 7.3665 ±0.0001 Å.

TABLE 2. Powder diffraction data analysis of the Cascadia Margin sample at P = 5.6 MPa, T = 85K. In the 2θ range 1.6 to 30°, 78 discernible peaks are observed, of which 26 are due to ice Ih and 52 are due to sI.

Ice Ih			Structure I		
(hkl)	d_{hkl}	I	(hkl)	d_{hkl}	I
(100)	3.9125	888	(110)	8.4382	42
(002)	3.6635	82	(200)	5.9569	22
(101)	3.4538	380	(210)	5.3304	89
(102)	2.6794	165	(211)	4.8611	91
(110)	2.2584	166	(310)	3.7651	10
(103)	2.0776	206	(222)	3.4406	205
(200)	1.9561	21	(320)	3.3001	68
(112)	1.9252	125	(321)	3.1786	357
(201)	1.8817	77	(400)	2.9734	46
(202)	1.7276	12	(410)	2.8871	98
(203)	1.5288	38	(330)	2.8061	67
(210)	1.4792	12	(421)	2.5966	43
(211)	1.4501	7	(332)	2.5369	9
(114)	1.4228	5	(430)	2.3795	6
(105)	1.3731	10	(510)	2.3349	4
(212)	1.3649	6	(520)	2.2092	19
(300)	1.3048	7	(530)	2.0408	53
(213)	1.2663	20	(531)	2.0106	31
(302)	1.2291	5	(442)	1.9841	14
(106)	1.1681	7	(532)	1.9305	58
(220)	1.1297	3	(620)	1.8908	29
(222)	1.0796	2	(540)	1.8588	8
(116)	1.0776	3	(444)	1.7171	1
(311)	1.0737	1	(552)	1.6193	2
(215)	1.0395	<1	(650)	1.5237	3
(313)	0.9924	7	(651)	1.5119	5
			(652)	1.4648	5
			(820)	1.4431	1
			(742)	1.4324	3
			(822)	1.4027	2
			(830)	1.3938	2
			(831)	1.3832	7
			(751)	1.3773	24
			(840)	1.3306	1
			(833)	1.3225	1
			(753)	1.3133	2
			(655)	1.2832	3
			(850)	1.2661	10
			(843)	1.2612	3
			(851)	1.2543	10
			(844)	1.2093	1
			(853)	1.2022	2
			(1000)	1.1963	2
			(950)	1.1554	1
			(953)	1.1096	1
			(864)	1.0964	1
			(865)	1.0648	4
			(963)	1.0601	1
			(1130)	1.0477	2
			(882)	1.0357	17
			(1132)	1.0278	4
			(1062)	1.0149	4
a = 4.5115 ±0.0068 Å,			a = 11.91132 ±0.0235 Å		
c = 7.3566 ±0.0001 Å			V = 1689.955 Å^3		
c/a = 1.6306 ±0.0001 Å					
V = 129. 672 Å^3					

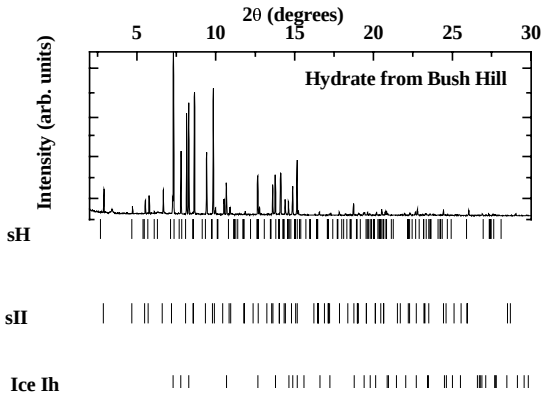

FIG. 3. Powder diffraction pattern for the hydrate sample from Bush Hill, Gulf of Mexico. Major structures of the sample are ice Ih and hydrate sII.

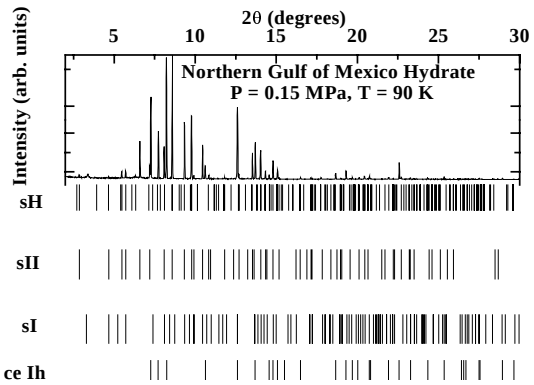

FIG. 4. Powder diffraction pattern for the hydrate sample from Green Canyon, northern Gulf of Mexico. Major structures of the sample are ice Ih and hydrate sII. A major conclusion gleaned from the powder pattern is that the quantity of hydrate in the sample is much more than that of ice.

The lattice parameter of sII is a = 17.2170 ±0.0060 Å. Though we observe that the Green Canyon samples consist mostly of sII and ice Ih, there are several peaks that could have an origin in sI (a = 11.9292 ±0.0380 Å) and sH (a = 11.7284 ±0.0451 Å and c = 9.6717 ±0.0001 Å) (see Table 4).

Discussion

In the present study, an attempt has been made to make structural studies of the natural minerals of gas hydrates. High-resolution angle-dispersive x-ray diffraction measurements were done at BESSRC beamline station 11-ID-D at the APS. It has been found that the gas hydrate samples from the Cascadia Margin consist of structure sI and ice Ih, while those from Bush Hill and the Green Canyon have sII and ice Ih in addition to sH. Ice Ih is found to coexist in all the natural minerals. The differences in the concentrations of sI, sII, and sH in these three samples point to the fact that the types of natural gases and their concentrations at geographically separate locations are very different. Stronger ice peaks in the Cascadia Margin samples point to the fact that the samples have a smaller concentration of hydrate. In contrast, the Bush Hill and Green Canyon samples contain more than 60% hydrates.

Acknowledgments

We are grateful to B.B. Rath, Associate Director, U.S. Naval Research Laboratory, for encouragements and exciting discussions. Also, we acknowledge the help of J.A. Linton, Materials Science Division, Argonne National Laboratory, in setting up the experiments. Use of the APS was supported by the U.S. Department of Energy, Office of Science, Office of Basic Energy Sciences, under Contract No. W-31-109-ENG-38.

References

[1] R.B. Coffin, R. Lamontagne, S. Rose-Pehrsson, K.S. Grabowski, D.L. Knies, S.B. Qadri, J.P. Yesinowski, J.W. Pohlman, M. Yousuf, and J.A. Linton, *2002 NRL Review* (U.S. Naval Research Laboratory, Washington, DC) p. 112 (2002).

[2] M. Yousuf, S.B. Qadri, D.L. Knies, K.S. Grabowski, R.B. Coffin, and J.W. Pohlman, Appl. Phys. A, on-line pub. DOI 10.1007/s0039-003-2091-y (2003).

[3] B.U. Haq, Science **285**, 543 (1999); J.M. Brooks, M.C. Kennicutt II, R.R. Fay, T.J. McDonald, and R. Sassen, Science **225**, 409 (1984).

[4] M.C. Kennicut II, J.M. Brooks, and G.J. Denoux, Marine Chem. **24**, 39 (1988).

[5] I.R. MacDonald, N.L. Guinasso, Jr., R. Sassen, J.M. Brooks, L. Lee, and K.T. Scott, Geology **22**, 699 (1994).

[6] R.K. McMullan and G.A. Jeffery, J. Chem. Phys. **42**, 2725 (1965).

[7] T.C.W. Mak and R.K. McMullan, J. Chem. Phys. **42**, 2732 (1965).

[8] K.A. Udachin and J.A. Ripmeester, Nature **397**, 420 (1999).

[9] J.A. Ripmeester and C.I. Ratcliffe, Energy Fuels **12**, 197 (1998).

[10] E.D. Sloan, Jr., Energy Fuels **12**, 191 (1998).

[11] W.S. Holbrook, H. Hoskins, W.T. Wood, R.A. Stephen, and D. Lizarralde, Science **273**, 1840 (1996).

[12] H. Shoji and C.C. Langway, Nature **298**, 548 (1982).

[13] Y.F. Makogon, T.Y. Makogon, and S.A. Holditch, in *Annals of the New York Academy of Sciences: Gas Hydrate: Challenges for the Future* **912**, 777, edited by G.D. Holder and P.R. Bishnoi (2000).

[14] H.-H. Rogner, Ann. Rev. Energy Environ. **22**, 217 (1997).

[15] R. Sassen, I.R. McDonald, A.G. Requejo, N.L. Guinasso, Jr., M.C. Kennicutt II, S.T. Sweet, and J.M. Brooks, Geo-Marine Lett. **14**, 110 (1994).
[16] L. Pauling, *The Nature of the Chemical Bond and The Structure of Molecules and Crystals* (Cornell University Press, Ithaca, NY) (1960).
[17] G.A. Jeffrey, *Inclusion Compounds, Vol. 1*, edited by J.L. Atwood, J.E.D. Davies, and D.D. MacNichol (Academic Press, London, 1984) p. 135.
[18] E.D. Sloan, Jr., *Clathrate Hydrates of Natural Gases* (Marcel Dekker, Inc., New York, NY, 1998).
[19] A. Rahman and F.H. Stillinger, J. Am. Chem. Soc. **95**, 7943 (1973).
[20] A. Khan, Chem. Phys. Lett. **253**, 299 (1996).
[21] M.A. Beno, C. Kurtz, A. Munkholm, U. Rüt, M. Engbretson, G. Jennings, J. Linton, G.S. Knapp, and P.A. Montano, Nucl. Instrum. Methods A **467-468**, 694 (2001).
[22] C. Gutt et al., Europhysics Lett. **48**, 269 (1999).

TABLE 3. Powder diffraction data analysis of the Bush Hill sample at P = 45 MPa, T = 93K. In the 2θ range 1.6° to 30°, 101 discernible peaks are observed, of which 27 are due to ice Ih, 45 are due to sII, and the remaining 22 and 7 peaks can be assigned correspondingly to sH and sI.

Ice Ih			Structure I			Structure II			Structure H		
(hkl)	d_{hkl}	I	(hkl)	d_{hkl}	I	(hkl)	d_{hkl}	I	(hkl)	d_{hkl}	I
(100)	3.8825	780	(110)	8.2947	36	(111)	9.7596	88	(201)	4.6787	7
(002)	3.6435	206	(421)	2.6057	16	(222)	6.0195	39	(102)	4.5076	9
(101)	3.4354	245	(1000)	1.1809	3	(311)	5.1375	44	(202)	3.6656	93
(102)	2.6622	104	(865)	1.0559	4	(222)	4.9308	26	(003)	3.4133	41
(110)	2.2477	213	(882)	1.0349	6	(400)	4.2615	105	(303)	2.4285	2
(103)	2.0657	131	(1132)	1.0257	1	(331)	3.9166	71	(544)	1.1841	2
(200)	1.9495	58	(1062)	0.9669	3	(422)	3.4860	424	(1000)	1.0521	1
(112)	1.9153	133				(333)	3.2881	640	(555)	1.0431	5
(201)	1.8804	213				(440)	3.0209	287	(627)	1.0203	1
(202)	1.7205	18				(531)	2.8904	628	(429)	0.9704	3
(203)	1.5232	60				(442)	2.8499	32			
(210)	1.4735	13				(620)	2.7051	60			
(211)	1.4545	14				(533)	2.6134	23			
(114)	1.4143	16				(622)	2.5797	6			
(105)	1.3718	21				(444)	2.4703	4			
(212)	1.3673	12				(711)	2.3972	14			
(300)	1.3005	10				(553)	2.2286	36			
(213)	1.2546	33				(800)	2.1394	3			
(302)	1.2254	9				(733)	2.0919	136			
(106)	1.1715	27				(644)	2.0696	99			
(220)	1.1259	5				(660)	2.0195	155			
(222)	1.0769	3				(822)	2.0158	91			
(311)	1.0657	8				(555)	1.9778	80			
(215)	1.0399	9				(842)	1.8693	18			
(313)	0.9896	10				(844)	1.7488	4			
						(666)	1.6490	10			
						(953)	1.5992	19			
						(1042)	1.5648	11			
						(11111)	1.5405	4			
						(1131)	1.4976	11			
						(1044)	1.4929	5			
						(1060)	1.4690	12			
						(973)	1.4449	8			
						(1200)	1.4284	4			
						(1064)	1.3827	2			
						(1082)	1.3228	1			
						(1155)	1.3113	5			
						(1173)	1.2817	13			
						(1084)	1.2786	4			
						(888)	1.2374	6			
						(1264)	1.2281	7			
						(1420)	1.2039	4			
						(1371)	1.1588	6			
						(1444)	1.1386	2			
						(999)	1.1003	22			

a = 4.5047 ±0.0037 Å,
c = 7.2412 ±0.0001 Å
c/a = 1.6075 ±0.0001 Å
V = 127.256 Å^3

a = 11.7346 ±0.0300 Å
V = 1615.844 Å^3

a = 17.0888 ±0.0040 Å
V = 4990.401 Å^3

a = 11.4496 ±0.3324 Å
c = 9.7064 ±0.0330 Å
c/a = 0.8478 ±0029
V = 1101.978 Å^3

TABLE 4. Powder diffraction data analysis of the hydrate sample from the northern Gulf of Mexico at P = 0.15 MPa, T = 90K. In the 2θ range 1.6° to 30°, 102 peaks are observed, of which 26 are due to ice Ih, 45 are due to sII, and the remaining 26 and 5 peaks can correspondingly be assigned to sH and sI.

Ice Ih			Structure I			Structure II			Structure H		
(hkl)	d_{hkl}	I	(hkl)	d_{hkl}	I	(hkl)	d_{hkl}	I	(hkl)	d_{hkl}	I
(100)	3.9134	293	(110)	8.4382	25	(111)	9.9722	9	(100)	10.1690	1
(002)	3.6767	161	(211)	4.8799	5	(220)	6.0947	7	(001)	9.6712	1
(101)	3.4555	396	(320)	3.3076	226	(311)	5.1963	24	(110)	5.8622	1
(102)	2.6803	58	(410)	2.9062	94	(222)	4.9744	22	(200)	5.0478	2
(110)	2.2592	309	(430)	2.3857	1	(400)	4.3066	47	(111)	5.0085	1
(103)	2.0777	128				(331)	3.9522	38	(002)	4.8799	5
(200)	1.9563	13				(422)	3.5179	92	(201)	4.4865	1
(112)	1.9252	61				(511)	3.3159	161	(102)	4.3804	1
(201)	1.8791	6				(440)	3.0435	184	(112)	3.6704	25
(202)	1.7285	7				(531)	2.9136	167	(300)	3.3778	20
(203)	1.5290	15				(442)	2.8699	12	(214)	2.0000	2
(210)	1.4788	23				(620)	2.7207	94	(510)	1.8229	1
(211)	1.4501	4				(533)	2.6259	15	(225)	1.6391	1
(114)	1.4203	7				(622)	2.5965	2	(008)	1.2087	1
(105)	1.3770	11				(551)	2.4104	6	(803)	1.1854	1
(212)	1.3722	4				(553)	2.2427	15	(550)	1.1764	4
(300)	1.3037	10				(800)	2.1519	2	(544)	1.1510	1
(213)	1.2663	43				(733)	2.1044	65	(635)	1.1045	3
(302)	1.2294	4				(660)	2.0296	108	(824)	0.9924	5
(106)	1.1764	4				(555)	1.9882	32	(627)	0.9699	1
(220)	1.1301	7				(842)	1.8791	32			
(222)	1.0789	5				(664)	1.8302	12			
(116)	1.0735	2				(951)	1.6652	5			
(311)	1.0697	2				(666)	1.6567	3			
(215)	1.0433	4				(953)	1.6060	7			
(313)	0.9924	4				(1042)	1.5724	2			
						(880)	1.5311	5			
						(955)	1.5050	2			
						(1060)	1.4766	4			
						(1133)	1.4607	4			
						(1200)	1.4350	1			
						(1064)	1.3973	12			
						(975)	1.3832	4			
						(991)	1.3485	2			
						(1082)	1.3282	3			
						(1155)	1.3170	2			
						(1173)	1.2873	3			
						(1084)	1.2837	1			
						(1333)	1.2598	10			
						(888)	1.2431	3			
						(1351)	1.2333	2			
						(1371)	1.1606	1			
						(1444)	1.1413	1			
						(999)	1.1047	3			
						(12122)	1.0100	2			
Ice Ih: 26 peaks a = 4.5170 ±0.0032 Å c = 7.3665 ±0.0001 Å c/a = 1.6308 ±0.0001 Å V = 130.162 Å^3			sI: 5 peaks a = 11.9292 ±0.0380 Å V = 1697.604 Å^3			sII: 45 peaks a = 17.2170 ±0.0060 Å V = 5103.538 Å^3			sH: 26 peaks a = 11.7284 ±0.0451 Å c = 9.6717 ±0.0001 Å c/a = 0.8246 ±0001 V = 1152.148 Å^3		